◆ Human Brain Mapping 37:3707–3720 (2016) ◆

Function–Structure Connectivity in Patients with Severe Brain Injury as Measured by MRI-DWI and FDG-PET

J. Annen,[1,2,3,†] L. Heine,[1,2,3,†] E. Ziegler,[1] G. Frasso,[4] M. Bahri,[1] C. Di Perri,[1,2] J. Stender,[5] C. Martial,[1,2,3] S. Wannez,[1,2,3] K. D'ostilio,[6] E. Amico,[1,2] G. Antonopoulos,[1,2] C. Bernard,[3] F. Tshibanda,[3] R. Hustinx,[3] and S. Laureys[1,2,3]*

[1]*Cyclotron Research Centre, University of Liège, Liège, Belgium*
[2]*Coma Science Group, GIGA Consciousness, University of Liège, Liège, Belgium*
[3]*University Hospital of Liège, Liège, Belgium*
[4]*Faculty of Social Sciences, Quantitative Methods for Social Sciences, University of Liège, Liège, Belgium*
[5]*University of Copenhagen, Copenhagen, Denmark*
[6]*Headache Research Unit, University of Liège, Liège, Belgium*

Abstract: A vast body of literature exists showing functional and structural dysfunction within the brains of patients with disorders of consciousness. However, the function (fluorodeoxyglucose FDG-PET metabolism)–structure (MRI-diffusion-weighted images; DWI) relationship and how it is affected in severely brain injured patients remains ill-defined. FDG-PET and MRI-DWI in 25 severely brain injured patients (19 Disorders of Consciousness of which 7 unresponsive wakefulness syndrome, 12 minimally conscious; 6 emergence from minimally conscious state) and 25 healthy control subjects were acquired here. Default mode network (DMN) function–structure connectivity was assessed by fractional anisotropy (FA) and metabolic standardized uptake value (SUV). As expected, a profound decline in regional metabolism and white matter integrity was found in patients as compared with healthy subjects. Furthermore, a function–structure relationship was present in brain-damaged patients between functional metabolism of inferior-parietal, precuneus, and frontal regions and structural integrity of the frontal-inferiorparietal, precuneus-inferiorparietal, thalamo-inferioparietal, and thalamofrontal tracts. When focusing on patients, a stronger relationship between structural integrity of thalamo-inferiorparietal tracts and thalamic metabolism in patients who have emerged from the minimally conscious state as compared with patients with disorders of consciousness was found. The latter finding

Additional Supporting Information may be found in the online version of this article.

Contract grant sponsor: University and University Hospital of Liège, the Belgian National Funds for Scientific Research (FRS-FNRS) the French Speaking Community Concerted Research Action (ARC - 06/11 - 340); Contract grant sponsor: NSERC discovery grant, IAP research network P7/06 of the Belgian Government (Belgian Science Policy); Contract grant sponsor: the European Commission; Contract grant sponsor: the James McDonnell Foundation, Mind Science Foundation; Contract grant sponsor: the European space agency (ESA); Contract grant sponsor: the Public Utility Foundation 'Université Européenne du Travail', "Fondazione Europea di Ricerca Biomedica."

*Correspondence to: Prof. Steven Laureys; Coma Science Group, CHU Sart Tilman, GIGA-Research B34-Quartier Hôpital, Avenue de l'Hôpital, 11, 4000 Liège, Belgium. E-mail: coma@chu.ulg.ac.be
†J. Annen and L. Heine have contributed equally to this work.

Received for publication 10 February 2016; Revised 12 April 2016; Accepted 16 May 2016.
DOI: 10.1002/hbm.23269
Published online 6 June 2016 in Wiley Online Library (wileyonlinelibrary.com).

was in line with the mesocircuit hypothesis for the emergence of consciousness. The findings showed a positive function–structure relationship within most regions of the DMN. *Hum Brain Mapp 37:3707–3720, 2016.*

Key words: FDG-PET; DWI; disorders of consciousness; function–structure coupling; default mode network

INTRODUCTION

Massive brain trauma can result in a disorder of consciousness (DOC), such as the unresponsive wakefulness syndrome (UWS) [Laureys et al., 2010], or minimally conscious state (MCS) [Giacino et al., 2002]. Patients who have emerged from MCS (EMCS) are able to functionally communicate and/or functionally use objects, but remain severely handicapped and dependent on full-time care. A substantial body of literature exists on grey matter metabolic (e.g., Fluorodeoxyglucose PET [FDG-PET]) and white matter structural (e.g., MRI-DWI [diffusion-weighted imaging]) brain characteristics in this patient group. Both these methods independently show severe impairments in DOC and EMCS patients [for review see Laureys and Schiff, 2012]. At a global level, functional measures show that metabolism in DOC patients is decreased by up to 40%–50% from their normal value [De Volder et al., 1997; Laureys et al., 1999b; Laureys et al., 2004; Rudolf et al., 1999; Tommasino et al., 1995]. Regional metabolic dysfunction is seen in a widespread frontoparietal, thalamocortical network. The medial part of this frontoparietal network, often called the default mode network (DMN), encompasses midline anterior cingulate/mesio-frontal and posterior cingulate/precuneal associative cortices as well as posterior parietal areas [Nakayama et al., 2006; Thibaut and Bruno, 2012]. In patients with disorders of consciousness, metabolic activity as well as MRI functional connectivity are reportedly more reduced in these regions than in the rest of the brain [Boly et al., 2009; Demertzi et al., 2014; Soddu et al., 2012; Vanhaudenhuyse et al., 2010a).

While the DMN is defined in terms of functional connectivity, there are indications of clear structural underpinnings [Greicius et al., 2009; Van Den Heuvel et al., 2009]. In patients with DOC, these structural connections are known to be damaged. For example, fractional anisotropy (FA), a measure of directionality of water diffusion assumed to be related to myelination of white matter, is specifically reduced in the DMN [Fernández-Espejo et al., 2011, 2012; Gomez et al., 2012].

The cerebral metabolic reductions in DOC are proposed to result from widespread neuronal injury [Thibaut and Bruno, 2012] or disruption of central excitatory drivers [Schiff, 2010]. The latter mesocircuit hypothesis proposes that large-scale dysfunction is due to an important reduction of thalamic excitatory output to the cortex. The observations of impaired metabolism suggest that axonal deafferentiation may be a key driver. We here aim to explore this DMN function–structure relationship in severely brain-damaged patients with varying levels of consciousness as measured by metabolism (standardized uptake value [SUV]) and white matter structural integrity (fractional anisotropy [FA]).

METHODS

Population

PET and MRI data from patients and 25 healthy controls were acquired at the University Hospital of Liège, Belgium. Patients were excluded from this study when pre-insult neurological illness, non-compatibility with either MRI or PET was present, or when less than 18 years. Behavioural diagnosis was determined by multiple coma recovery scale revised [CRS-R's; Giacino et al.,] assessments, including assessments on both MRI and PET scan dates. Written informed consent was taken from each healthy subject and the legal guardians of each patient in accordance with the Declaration of Helsinki. The Ethics Committee of the University Hospital of Liège approved the study.

Data Acquisition

MRI data was acquired using a 3 Tesla scanner (Siemens Trio, Siemens Medical Solutions, Erlangen, Germany). Structural MRI T1 data were obtained with T1-weighted 3D gradient echo images using 120 slices, repetition time = 2,300 ms, echo time = 2.47 ms, voxel size = 1 × 1 × 1.2 mm^3, flip angle = 9°, field of view = 256 × 256 mm^2. Diffusion-weighted images were acquired at a b-value of 1,000 s/mm^2 using 64 encoding gradients that were uniformly distributed in space by an electrostatic repulsion approach [Jones et al., 1999]. Voxels had dimensions of 1.8 × 1.8 × 3.3 mm^3, field of view = 230 × 230 mm^2, repetition time = 5,700 ms, echo time = 87 ms, and volumes were acquired in 45 transverse slices using a 128 × 128 voxel matrix. A single unweighted ($b = 0$) image preceded the diffusion-weighted volumes and the 64-volume diffusion imaging sequence was repeated twice.

Five days prior to MRI, an ^{18}F-FDG PET scan was performed 52 ± 13 minutes after intravenous injection of 300 ± 47 MBq of FDG using a Gemini TF PET-CT scanner (Philips Medical Systems). A low-dose CT was acquired

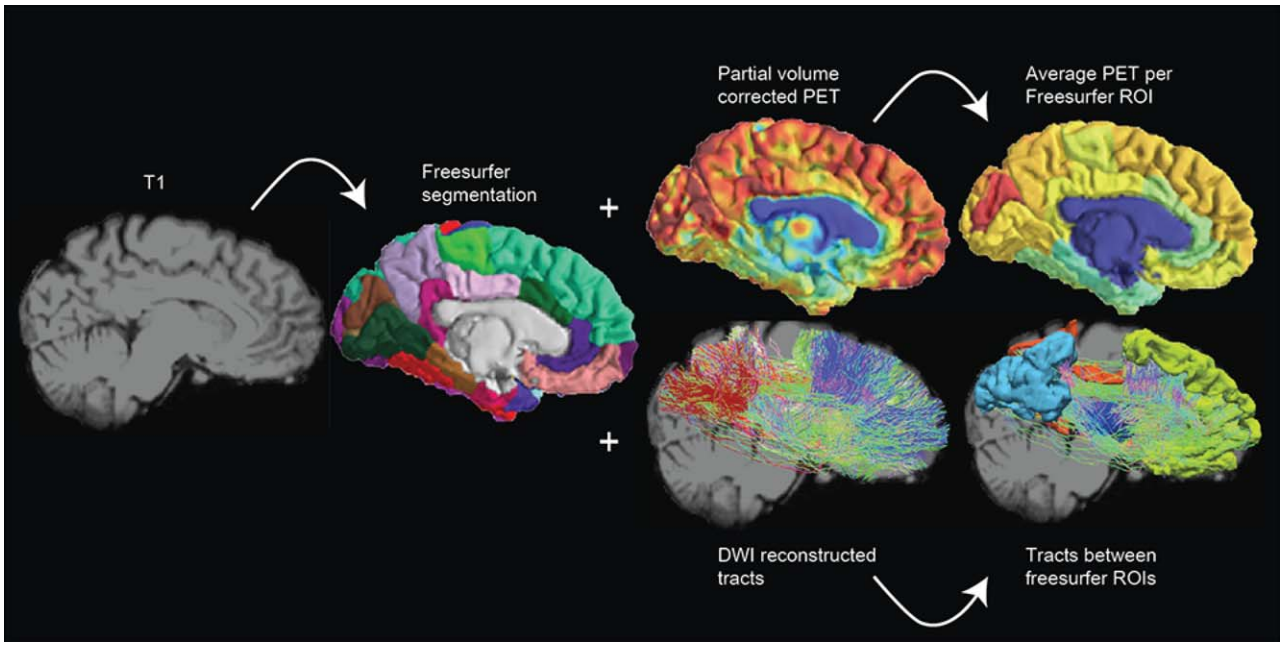

Figure 1.

Schematic representation of the processing pipeline. Data was assessed in subject space where the T1 MRI was segmented using Freesurfer. PET glucose metabolism was estimated by calculation of mean partial volume corrected standardized uptake values within the default mode network ROIs. FA was extracted of the voxels that the DMN tract passed through. [Color figure can be viewed at wileyonlinelibrary.com]

for attenuation correction, followed by a 12-minute emission scan. The studies were reconstructed using a LOR-OSEM algorithm and reconstructed images had 2 mm^3 isotropic voxels in a 256 × 256 × 89 voxel matrix.

Data Processing

The images of each subject were manually reoriented to the orientation of the MNI 152 1 mm^3 template. Next, each subject's T1-weighted image was automatically labelled using the Desikan–Killiany atlas via the processing pipeline of Freesurfer v 5.3.0 [Desikan et al., 2006]. Several preselected region labels were combined to produce eight regions of interest representing the DMN in both hemispheres. Specifically, regions of interest (ROIs) in the left and right thalamus, inferior parietal cortex, mesio-frontal cortex (encompassing: medial orbital frontal, superior frontal, and rostral anterior cingulate cortex), and precuneus/posterior cingulate cortex (encompassing: precuneus, isthmus, and posterior cingulate cortex) were targeted. Figure 1 shows an example of the processing protocol adopted. The Freesurfer processing pipeline was also used to segment the entire cerebrum into distinct grey matter (GM), white matter (WM), and cerebrospinal fluid (CSF) images.

Because the processing of damaged brains is slightly inconsistent across neuroimaging toolboxes, we additionally segmented each T1-weighted image into whole-brain WM, GM, and CSF masks using FAST, part of FSL (FMRIB Software Library v 5.0) [Smith et al., 2004]. A robust cerebral white matter mask was obtained for each subject by multiplying the WM masks produced by the FAST and Freesurfer toolbox. Subsequently, a reliable cerebral brain mask for tractography termination was produced by multiplying the cerebrum mask calculated by Freesurfer (including all cortical brain matter) with the inverse of the FAST cerebrospinal fluid mask. This procedure helped to minimize contamination of masks with non-brain tissue that had been incorrectly labelled.

Diffusion-weighted images were corrected for subject motion by rigid registration of the weighted volumes to the unweighted volume. Rotations applied to the diffusion-weighted volumes were also applied to the corresponding gradient directions [Leemans and Jones, 2009]. Distortion artefacts induced by eddy currents were then corrected by affine registration of the diffusion-weighted images to the unweighted volume. All registrations were performed with FLIRT, part of FSL. The data of some subjects was contaminated by table vibration artefacts which have previously been reported for this model of MR scanner [Gallichan et al., 2010]. The artefact manifested as extraordinarily high diffusion in the left-to-right direction that was clearly visible in calculated RGB-FA images. In our sample it was found primarily in posterior brain areas,

though its effects occasionally appeared throughout the brain. We reduced the effect of the artefact by removing volumes in which the absolute value of the x-component of the encoding gradient vector exceeded a manually selected threshold. This threshold was chosen by repeatedly examining the RGB-FA image at distinct thresholds by at least two assessors.

For both analysis and preprocessing diffusion tensors were fit at each voxel using non-linear least squares fitting. Tensor eigenvalues were constrained to positivity by taking their absolute value. This method is known to be robust against noise [Koay, 2009]. FA, tensor mode [Ennis and Kindlmann, 2006], and RGB-FA images were computed. Tensor mode provides a method for quantifying the type of anisotropy (e.g., planar = two fibre populations, or linear = one fibre population) found in the voxel. Mode ranges between −1 (planar anisotropy) and +1 (linear anisotropy) with 0 representing orthotropy. All tensor calculations were performed with Dipy [Garyfallidis et al., 2014].

Affine registration was performed between each subject's white matter mask (in T1 space) and a thresholded FA image ($FA > 0.2$) using FLIRT (nearest neighbour interpolation, mutual information cost function), part of FSL. The translation component of the transformation matrix was modified by adding half of the difference between the fields of view of the DWI and T1-weighted images. This allows the transformation matrix to be used to register T1-derived masks to those in DWI orientation without downsampling. The transformation matrix was applied to the T1-derived white matter mask, cerebral track termination mask, and ROI label map.

A set of voxels with unidirectional diffusion (or a "single fibre population") was identified by eroding and thresholding ($0.8 < FA < 0.99$) the FA image and multiplying this by a map of the thresholded tensor mode (mode > 0.9). These operations were performed with fslmaths, part of FSL. Binary single fibre population masks were manually revised to select only voxels that were clearly inside the corpus callosum and corticospinal tracts. These high FA and high mode voxels were used to estimate the diffusion-weighted signal response for a single fibre population. Next, non-negativity constrained spherical deconvolution was performed and fibre orientation distribution functions within each voxel were estimated. A maximum harmonic order of 4 was used for both response estimation and spherical deconvolution. Probabilistic tractography was performed using randomly placed seeds within the subject-specific white matter masks described above. Fibre tracking settings were as follows: number of tracks = 1,000,000, FOD magnitude cutoff for terminating tracks = 0.1, minimum track length = 10 mm, maximum track length = 200 mm, minimum radius of curvature = 1 mm, tracking algorithm step size = 0.2 mm. Streamlines were terminated when they (i) extended out of the cerebrum track termination mask, or (ii) could not progress along a direction with FOD magnitude or curvature radius higher than the minimum cutoffs. A connectivity matrix for the eight-region connectome was computed using the streamline origin and termination points and the ROI label mask. For each streamline the FA was averaged over all the voxels it passed through; meaning that we extracted the FA within the 12 tracts connecting each of our DMN regions of interest. Constrained spherical deconvolution and fibre tracking were performed with MRtrix 0.2.12 [Tournier et al., 2012]. Computation of the connectivity matrices was performed with MRtrix 0.3.

FDG-PET images for each subject were first manually reoriented toward the T1-weighted image using Statistical Parametric Mapping 8 (SPM8; www.fil.ion.ucl.ac.uk/spm) in order to ease later automated registration tasks. FDG-PET images underwent partial volume effect (PVE) correction using the Muller–Gartner–Rousset method [Müller-Gärtner et al., 1992; Rousset et al., 2007] in PVElab v 2.2 [Quarantelli et al., 2004; Svarer et al., 2005]. Partial volume correction aims to remove the spillover of signal to regions that are known to be without activity (e.g., CSF), in order to prevent underestimation of signal in regions with activity (e.g., GM). Grey matter, white matter, and cerebrospinal fluid partial volume estimate images were obtained, as earlier, using FAST. A rigid-body transformation was obtained between the uncorrected FDG-PET and the subject's T1-weighted image to bring the T1 image to PET space (trilinear interpolation, correlation ratio cost function; in six patients, cost function was changed to normalized mutual information to improve registration). The inverse of this transformation matrix was applied to the GM, WM, and CSF partial volume images to bring them into the space of the PET image. The point spread function was modelled by 3D Gaussian function with in-plane full-width at half maximum (FWHM) values of 8 mm. Finally, following PVE correction the PET image was transformed into T1 space and the mean SUV value was extracted within each ROI using in-house software.

For all subjects it was necessary to manually check the performance of the automated labelling and registration procedures. In six patients there were voxels that were clearly mislabelled and required correction. The ROI labels were evaluated and adjusted when deemed necessary by at least two researchers. Processing pipelines were developed in Python using Nipype [Gorgolewski et al., 2011] and are freely available online (https://github.com/GIGA-Consciousness/structurefunction). A figure showing ROIs and tracts can be found in the Supporting Information Fig. 1.

Statistical Analysis

Statistical analysis was done using R [R Core Team, 2014]. First, to test for demographic differences (age and gender) between our two groups (healthy controls and brain-injured patients), we used independent two-sample *t*-tests or chi-square test, respectively. To test for possible differences between left and right brain function/structure

we assessed laterality differences using a two sample *t*-tests within brain-injured patients and controls with a "logit" transform of FA and log transformation of SUV to account for parametric test-assumptions. Subsequently, SUV and FA of the left and right hemisphere regions were averaged for each subject. Next, to test the differences between the two groups in mean SUV and FA values two-sample *t*-tests with Bonferroni correction ($\alpha = 0.012$ and $\alpha = 0.008$ respectively) were used. Using a χ^2 test the number of volumes removed during vibration artefact correction was evaluated to identify any potential group bias. Subsequently, multivariate linear regression analysis with group and FA as regressors was performed to model how group and structural integrity (FA) of DMN tracts relate to metabolism (SUV) in adjacent regions. SUV was log scaled to meet normality assumptions. Furthermore, to take into account the differences in variance we weighted the regression function by the inverse of the FA of the corresponding connection. Type II ANOVA's were used to assess significant main and interaction effects. As each SUV ROI is tested three times, Bonferroni correction was used with $\alpha = 0.016$.

We then focused on patients alone to better understand the structure–function relationship in the brain-injured group. Multiple linear regression models were used to investigate how demographic factors as diagnosis (DOC vs. EMCS), aetiology (TBI or non-TBI), disease duration (subchronic vs. chronic), gender, and age influence the function–structure relationship in the patient population. Type II ANOVA's were used to assess significant main and interaction effects. Within the control population we tested for an effect of FA on SUV using a simple linear regression with FA as regressor and SUV as outcome measure.

To assess a possible global effect of SUV and FA we used a multivariate linear regression analysis to model how group and whole-brain structural integrity of white matter (FA over all white matter voxels) relate to whole-brain grey matter metabolism (SUV). Furthermore we performed an analogous regression analysis for the patient and control group separately.

RESULTS

We obtained MRI data of 163 adult, (sub-) chronic (>30 days after injury) patients without pre-existing comorbidities and 14 healthy control subjects between November 2009 and October 2013. Stringent exclusion criteria were applied as visualized in Fig. 2. Patients were excluded because of technical difficulties in either MRI or PET ($N = 25$), more than 5 days between exams ($N = 5$), severe deformations consisting of more than one-third of one hemisphere (e.g., enlarged ventricles, haemorrhage, severe atrophy), metal/drain artefacts ($N = 79$). Data of 54 patients were preprocessed, although 29 subjects had to be excluded because Freesurfer was unable to complete segmentation. Thus, the final cohort consisted of 25 patients and 25 healthy controls. The patients did not differ from control subjects in age ($P = 0.214$; mean age = 36.3 for brain injured and 40.9 for healthy controls) or gender ($P = 0.756$; 13 male against 11 male in brain injured and healthy groups, respectively).

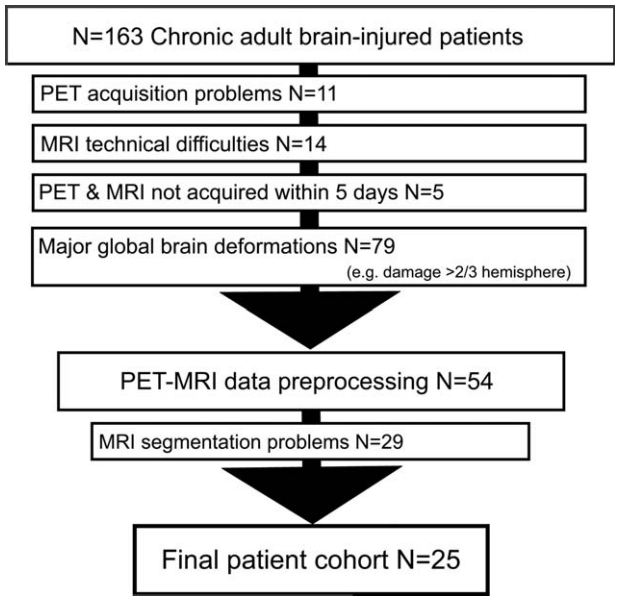

Figure 2.
Flowchart of exclusion criteria. This study was conducted using stringent exclusion criteria. Of the 163 MRI examinations performed at the Coma Science Group between November 2009 and October 2013, 109 were excluded before image analysis. Data preprocessing was done for 54 patients, of which additionally 19 subjects had to be excluded due to inaccurate segmentation. Finally, we included 25 patients in the statistical analysis.

DOC patients had been clinically diagnosed as in an unresponsive wakeful state (UWS, $n = 7$) or a minimally conscious state (MCS, $n = 12$), and diagnosis was consistent with the diagnosis of the day of the PET and MRI scan. Six subjects were diagnosed as emerged from a minimally conscious state (EMCS, $n = 6$). The patient cohort consisted of subacute ($n = 10$, between 30 days and 3 months after onset) and chronic patients ($n = 15$, >3 month after onset) with a mean time since onset of 1.8 years (SD = 1.9 years). Patients suffered from traumatic brain injury (TBI, $n = 12$), anoxia ($n = 11$), both (mix, n = 1), or infection ($n = 1$). For demographic and clinical details see Table I.

The vibration artefact affected 14 of 25 patients and 5 out of 25 controls. On average, 39 diffusion-weighted volumes (30%) had to be removed from patient data and 32 (25%) out of 128 volumes from control subjects. We did not find a difference between the amount of affected volumes between patients and controls [$\chi^2(1,N = 50) = 3.14$, $P = 0.076$].

TABLE I. Patient demographics

Diagnosis	Age	Gender	Etiology	Days (Onset)	GOSE	CRS-R A.	CRS-R V.	CRS-R M.	CRS-R O.	CRS-R C.	CRS-R Ar.	CRS-R total
EMCS	33	F	TBI	388	NA	4	5	6	3	2	3	23
EMCS	30	M	TBI	881	3	4	5	6	3	2	3	23
EMCS	37	M	Anoxia	284	3	4	5	6	3	0	2	20
EMCS	45	F	Anoxia	38	3	4	5	6	3	1	1	20
EMCS	31	F	TBI	439	3	4	5	5	2	2	2	20
EMCS	22	M	TBI	2,424	3	3	4	6	3	1	1	18
MCS+	28	M	TBI	589	3	1	2	2	1	0	1	7
MCS+	45	M	TBI	533	3	3	3	3	1	0	2	12
MCS+	47	F	Anoxia	210	NA	3	0	1	1	0	2	7
MCS+	19	M	MIX	1,236	3	3	4	1	2	0	2	12
MCS+	23	M	TBI	752	3	3	4	5	1	0	2	15
MCS+	48	F	Anoxia	292	NA	3	1	2	2	0	1	9
MCS+	49	M	Anoxia	674	1	3	1	3	1	0	2	10
MCS-	29	F	TBI	569	3	1	2	1	2	0	1	7
MCS-	28	M	TBI	634	2	0	1	2	1	1	1	6
MCS-	36	F	Anoxia	549	3	1	3	2	2	1	1	10
MCS-	45	F	Anoxia	259	1	0	0	2	1	0	1	4
MCS-	48	M	Anoxia	1,100	3	1	3	1	2	0	1	8
UWS	40	M	Anoxia	2,890	3	1	0	1	2	0	1	5
UWS	21	M	TBI	196	2	1	0	2	2	0	2	7
UWS	44	F	Anoxia	101	1	0	0	2	1	0	1	4
UWS	54	F	Infection	51	1	0	0	2	1	0	1	4
UWS	20	M	TBI	31	7	0	1	2	1	0	1	5
UWS	48	F	Anoxia	129	1	1	0	0	1	0	2	4
UWS	37	F	TBI	1,192	3	1	0	1	1	0	2	5

EMCS, Emergence from minimally conscious state; MCS, minimally conscious state; UWS, unresponsive wakefulness syndrome; M, male; F, female; TBI, traumatic brain injury; MIX, anoxia and traumatic brain injury; GOSE, Glasgow outcome scale extended; CRS-R, Coma recovery scale – revised; A., Auditory; V., visual; M., motor; O., oromotor; C., communication; Ar., arousal.

To assess if there is an effect of laterality, the difference between SUV values in our ROIs and FA values for connections in the left and right hemisphere were assessed. No differences could be observed within SUV values for controls ($P = 0.794$) or patients ($P = 0.691$), nor in FA values between the left and right tracts (controls; $P = 0.156$, patients; $P = 0.053$). The values of each hemisphere were averaged for subsequent analysis so that each subject was not tested twice.

Functional and Structural Integrity

Metabolism (SUV values) was significantly ($P < 0.001$) lower in brain-injured patients compared with controls (Fig. 3). The average reduction in SUV of patients was 42%. The reduction was strongest in the precuneus (44%) and weakest in the frontal cortex (39%).

FA was also significantly ($P < 0.001$) lower in brain-injured patients compared with controls (Fig. 4). The average reduction of FA was 17%, with the biggest reduction in the fronto-precuneus tract (23%) and the smallest reduction in the thalamo-precuneus radiation (13%). A table indicating all two-sample *t*-tests with Bonferroni correction can be found in the Supporting Information.

Regression Analysis

Explaining SUV through FA and group

Multiple linear regression (Fig. 5; Supporting Information Fig. 2; Tables (II–V) for *P*-values) including the two groups (patients and controls) showed a main effect of FA and of group (with Bonferoni correction of $P < 0.016$). The main effect of group is significant for all the regions and adjacent tracts with a higher SUV for healthy controls than for patients, except for SUV in the inferioparietal cortex with FA from the frontal to inferioparietal tract where only a trend can be observed.

The main effect of FA can be found in five tracts (Fig. 5). This is the case for SUV in the inferioparietal cortex and FA from all assessed tracts toward this ROI (thalamo-interioparietal $P < 0.0001$, frontal-inferioparietal $P = 0.012$, precuneus-inferioparietal $P < 0.0001$), SUV in the precuneus and precuneus-inferioparietal FA ($P < 0.0001$), and SUV of the frontal cortex and thalamo-frontal FA

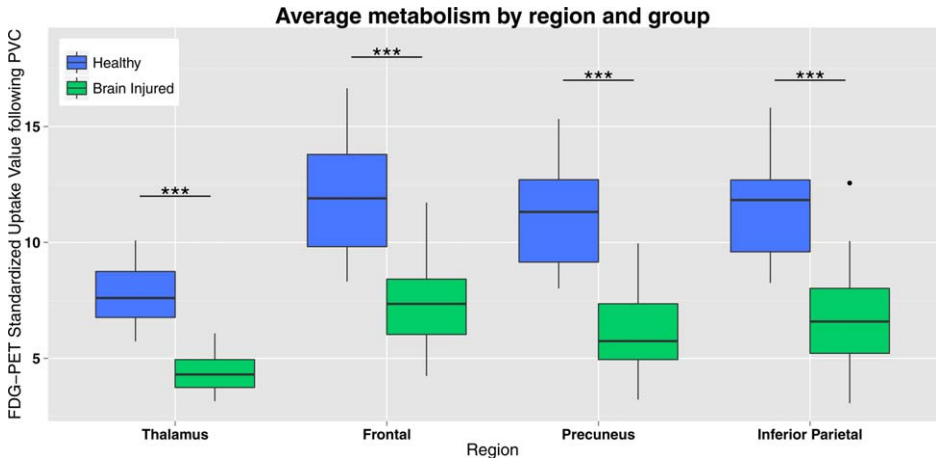

Figure 3.

PET glucose uptake in DMN regions. Standardized uptake value following partial volume correction (PVC) in the default mode network regions (average of standardized uptake values of left and right hemisphere) for healthy controls and brain injured patients. Brain injured patients show a decreased standardized uptake value compared with controls in all default mode network regions. *** = $P < 0.001$. [Color figure can be viewed at wileyonlinelibrary.com]

($P = 0.009$) (Tables II–V). The relationship between FA and SUV within each of the two samples has been further investigated and the results are discussed in the following paragraph.

Explaining SUV through FA and demographic factors

Within patients, we did not find any significant effect of aetiology (TBI or non-TBI), duration, gender, or age in the multiple linear regression model. An interaction effect between group (EMCS vs. DOC) and FA was found (with Bonferoni correction $\alpha < 0.016$) on thalamic SUV and thalamo-inferioparietal FA ($P = 0.006$). Trends were observed for thalamic SUV and the other two tracts toward this ROI (thalamo-frontal $P = 0.04$, thalamo-precuneus $P = 0.017$) (Supporting Information Fig. 4). Furthermore, apart from one, all observed main effects of FA seen in the previous analysis were also observed in the current analysis between the two patient populations. SUV in the inferioparietal cortex is explained by thalamo-

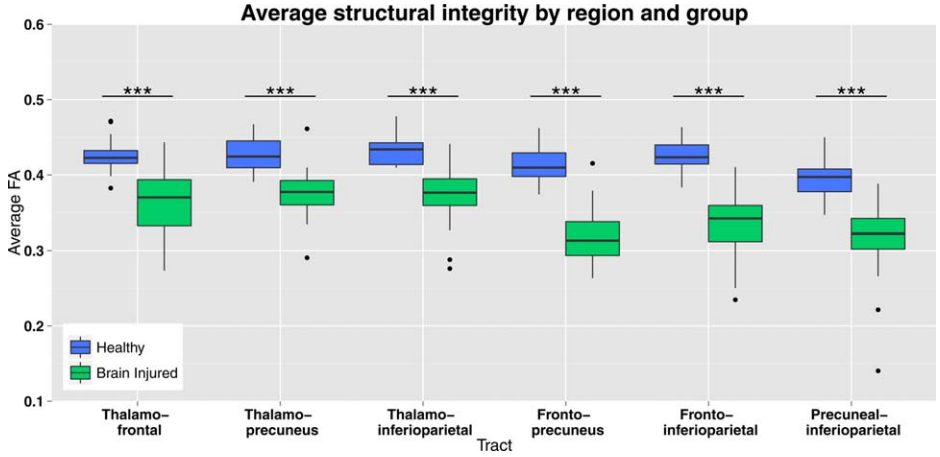

Figure 4.

MRI white matter structural integrity in DMN tracts. Structural integrity of tracts between the default mode network regions represented with FA of the voxels that the tracts pass through, in healthy controls and brain injured patients (average of left and right hemispheres). Brain injured patients show lower FA values compared with healthy controls subjects in all tracts. *** = $P < 0.001$. [Color figure can be viewed at wileyonlinelibrary.com]

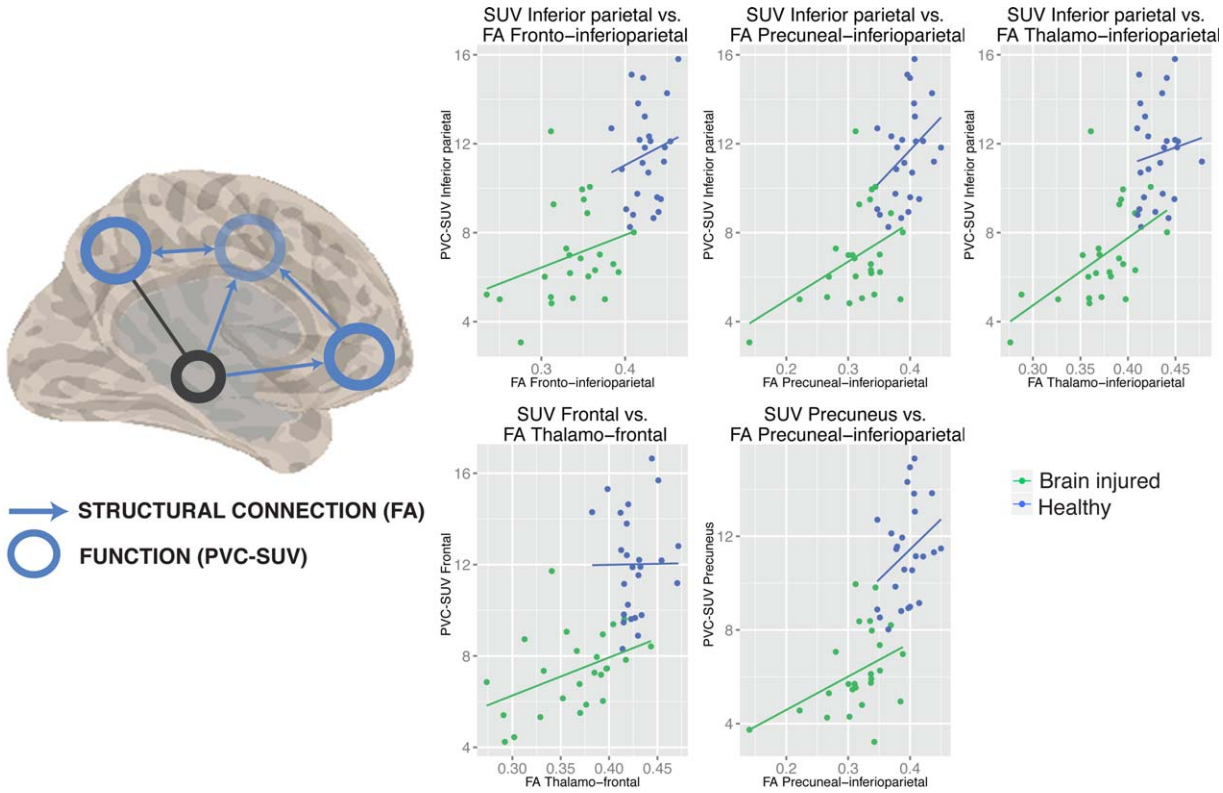

Figure 5.

Linear regression model of the function–structure relationship. Left side of the image shows a spatial representation of the function–structure relationships (*blue circles* for regions where the partial volume corrected - standardized uptake value (PVC-SUV) depended on FA, *blue arrows* for FA of tracts that drive SUV in adjacent regions). Right side of image shows five scatterplots of the linear regression models for healthy controls (*blue dots*), and patients (*green dots*), and significant main effect of FA (*lines*). Abbreviations: FA, fractional anisotropy; PVC-SUV, partial volume corrected-standardized uptake value. [Color figure can be viewed at wileyonlinelibrary.com]

interioparietal FA ($P = 0.002$), and precuneus-inferioparietal FA ($P < 0.0001$). Similarly, SUV in the precuneus that depends on the precuneus-inferioparietal FA ($P = 0.002$). SUV of the frontal cortex is linearly related to thalamo-frontal FA ($P = 0.012$). Within the healthy population there is no evidence for a main effect of FA on SUV in any of the structure–function pairs (Table VI).

Whole brain regression analysis

To test if these results were limited to the DMN or reflective of general brain integrity, we performed a linear regression analysis to model how group and whole-brain structural integrity of white matter (FA) relate to whole brain grey matter metabolism (SUV). This additional analysis showed a main effect of group ($P = 0.0003$), but not of FA ($P = 0.17$). Instead, a small evidence for an interaction effect could be observed ($P = 0.03$) (Supporting Information Fig. 3). However, we did not find evidence for a structure–function relationship within each subgroup.

DISCUSSION

We here aimed to directly investigate, in severely brain injured patients, the relationship between functional brain activity and structural connectivity within the DMN in an objective and combined fashion using both FDG-PET and FA MRI. We show that a function–structure relationship is present in brain-damaged patients between functional metabolism of inferior-parietal, precuneus, and frontal regions and structural integrity of the frontal-inferiorparietal, precuneus-inferiorparietal, thalamo-interioparietal and thalamofrontal tracts. When focusing on EMCS versus DOC patients, we found a stronger relationship between structural integrity of thalamo-inferiorparietal tracts and thalamic metabolism in patients who have emerged from MCS as compared with DOC patients.

We first assessed function (PET metabolism) and structure (DWI-FA) independently, to replicate previous studies focusing on either measure separately. Indeed, marked impairments in SUV and FA were observed in patients.

TABLE II. Regression analysis SUV of the thalamus, FA, and group (healthy vs. brain injured)

SUV	FA	R^2	Beta	95% confidence interval		Sum Sq	Df	F	P-value	
Thalamus	Thalamo-frontal	0.722								
	FA		0.538	−1.029	2.105	0.026	1	0.309	0.581	
	Group		0.947	−0.819	2.713	4.823	1	56.763	0.000	***
	Interaction		−0.988	−5.216	3.240	0.019	1	0.221	0.640	
	Residuals					3.908	46			
Thalamus	**Thalamo-inferiorparietal**	0.721								
	FA		0.523	−1.358	2.404	0.036	1	0.425	0.518	
	Group		0.425	−1.623	2.474	4.338	1	50.929	0.000	***
	Interaction		0.255	−4.591	5.101	0.001	1	0.011	0.916	
	Residuals					3.833	45			
Thalamus	**Thalamo-precuneus**	0.731								
	FA		1.322	−0.882	3.526	0.083	1	1.007	0.321	
	Group		1.100	−0.641	2.841	4.200	1	50.900	0.000	***
	Interaction		−1.411	−5.623	2.801	0.038	1	0.456	0.503	
	Residuals					3.713	45			

Statistics and confidence interval of the regression models to predict SUV using FA of adjacent tracts and group (brain-injured patients or healthy control subjects). * = $P < 0.05$, ** = $P < 0.01$, *** = $P < 0.00$.

SUV in all DMN regions was lowered in brain-injured patients compared with healthy controls, with a 39%–42% reduction of metabolic rates in brain-injured patients in the cortical DMN regions and thalamus (Fig. 3). This is in accordance with previous findings on a global brain scale [Laureys et al., 1999a,; Rudolf et al., 1999; Stender et al., 2014a,b; Tommasino et al., 1995] and within the DMN specifically [Fridman et al., 2014; Nakashima et al., 2007; Thibaut and Bruno, 2012]. FA in all DMN tracts was diminished by about 13%–23% in brain-injured patients compared with healthy controls (Fig. 4), in line with previous reports [Fernández-Espejo et al., 2011, 2012; Gómez et al., 2012]. Our results support recent findings of diminished structural integrity of corticocortical and subcorticocortical DMN connections, which correlated with clinical severity in a group of eight patients [Lant et al., 2015].

The main aim of this study was to assess the function–structure relationship in the DMN and thalamus in healthy conscious subjects and coma survivors. First, as expected, we have replicated previous studies and shown that patients have significantly lower FA in all studied connections and SUV in all regions. Building on this, we showed that grey matter metabolic function can be partially explained by white matter anisotropy in several regions of

TABLE III. Regression analysis SUV of the frontal cortex, FA, and group (healthy vs. brain injured)

SUV	FA	R^2	Beta	95% confidence interval		Sum Sq	Df	F	P-value	
Frontal	Thalamo-frontal	0.644								
	FA		2.692	0.860	4.524	0.872	1	7.510	0.009	**
	Group		1.502	−0.563	3.566	2.232	1	19.222	0.000	***
	Interaction		−2.732	−7.674	2.211	0.144	1	1.238	0.272	
	Residuals					5.342	46			
Frontal	**Frontal-inferiorparietal**	0.607								
	FA		2.254	0.253	4.255	0.688	1	5.090	0.029	*
	Group		0.836	−1.417	3.088	1.165	1	8.624	0.005	**
	Interaction		−1.254	−6.696	4.187	0.029	1	0.216	0.645	
	Residuals					6.081	45			
Frontal	**Frontal-precuneus**	0.587								
	FA		1.635	−0.754	4.024	0.133	1	0.926	0.341	
	Group		1.574	−0.487	3.635	1.685	1	11.736	0.001	**
	Interaction		−2.955	−8.174	2.264	0.187	1	1.299	0.260	
	Residuals					6.603	46			

Statistics and confidence interval of the regression models to predict SUV using FA of adjacent tracts and group (brain-injured patients or healthy control subjects). * = $P < 0.05$, ** = $P < 0.01$, *** = $P < 0.00$

TABLE IV. Regression analysis SUV of the precuneus, FA, and group (healthy vs. brain injured)

SUV	FA	R^2	Beta	95% confidence interval		Sum Sq	Df	F	P-value	
Precuneus	Thalamo-precuneus	0.675								
	FA		4.249	1.348	7.150	0.863	1	6.037	0.018	*
	Group		2.318	0.026	4.609	3.351	1	23.434	0.000	***
	Interaction		−4.503	−10.047	1.041	0.383	1	2.676	0.109	
	Residuals					6.434	45			
Precuneus	**Frontal-precuneus**	0.622								
	FA		1.865	−0.841	4.570	0.196	1	1.063	0.308	
	Group		1.692	−0.642	4.026	2.527	1	13.725	0.001	***
	Interaction		−3.018	−8.928	2.893	0.194	1	1.056	0.309	
	Residuals					8.468	46			
Precuneus	**Precuneus-inferioparietal**	0.720								
	FA		2.618	1.245	3.990	2.465	1	16.571	0.000	***
	Group		0.469	−1.037	1.976	3.393	1	22.810	0.000	***
	Interaction		−0.148	−4.068	3.772	0.001	1	0.006	0.940	
	Residuals					6.843	46			

Statistics and confidence interval of the regression models to predict SUV using FA of adjacent tracts and group (brain-injured patients or healthy control subjects). * = $P < 0.05$, ** = $P < 0.01$, *** = $P < 0.00$.

the DMN within the patient cohort. More specifically, metabolism of the frontal cortex, precuneus, and inferior parietal cortex can be explained by fronto-inferioparietal, precuneal-inferiorparietal, and thalamo-inferioparietal as well as thalamo-frontal structural integrity (FA). These results are in line with the limited previous studies indicating there might be a link between structural integrity and glucose metabolism. For example, one study correlating metabolism with white matter bundles in the DMN in healthy subjects found that working memory is related to a structure–function correlation in the cingulum [Yakushev et al., 2013]. Further studies have shown that diffusion measures have been correlated to glucose uptake in patients with Alzheimer's disease and dementia [Bozoki et al., 2012; Kuczynski et al., 2010; Yakushev et al., 2011], children with occipital lesions [Jeong et al., 2015], normal aging [Inoue et al., 2008], and epilepsy [Chandra et al., 2006]. However, all of these studies use simple correlations instead of regressions measures, and thus do not take population-specific changes into account. This could result in false positive-correlations, driven by main effects of group on the (in) dependent variables. We provide proof that metabolic function is indeed directly related to structural integrity, surpassing existing correlational results.

TABLE V. Regression analysis SUV of the inferioparietal cortex FA, and group (healthy vs. brain injured)

SUV	FA	R^2	Beta	95% confidence interval		Sum Sq	Df	F	P-value	
Inferior parietal	Thalamo-inferioparietal	0.683								
	FA		5.278	2.989	7.567	2.562	1	20.321	0.000	***
	Group		1.824	−0.668	4.317	1.075	1	8.528	0.005	**
	Interaction		−3.697	−9.593	2.199	0.201	1	1.595	0.213	
	Residuals					5.673	45			
Inferior parietal	**frontal-inferioparietal**	0.585								
	FA		2.961	0.680	5.241	1.216	1	6.928	0.012	*
	Group		0.863	−1.705	3.431	0.953	1	5.426	0.024	*
	Interaction		−1.395	−7.597	4.808	0.036	1	0.205	0.653	
	Residuals					7.901	45			
Inferior parietal	**Precuneus-inferioparietal**	0.668								
	FA		3.283	1.656	4.910	2.477	1	18.739	0.000	***
	Group		0.502	−1.020	2.023	1.400	1	10.591	0.002	**
	Interaction		−0.552	−4.525	3.421	0.010	1	0.078	0.781	
	Residuals					5.949	45			

Statistics and confidence interval of the regression models to predict SUV using FA of adjacent tracts and group (brain-injured patients or healthy control subjects). * = $P < 0.05$, ** = $P < 0.01$, *** = $P < 0.00$.

TABLE VI. Statistics and confidence interval of the regression models to predict SUV of the thalamus using FA of adjacent tracts and group (DOC patients and patients who recovered from DOC)

SUV	FA	R^2	Beta	95% confidence interval		Sum Sq	Df	F	P-value	
Thalamus	Thalamo-frontal	0.200								
	FA		0.270	−1.459	1.999	0.044	1	0.516	0.480	
	Group		−3.965	−7.742	−0.188	0.003	1	0.038	0.848	
	Interaction		10.299	0.456	20.142	0.401	1	4.735	0.041	*
	Residuals					1.777	21			
Thalamus	**Thalamo-inferiorparietal**	0.333								
	FA		−0.282	−2.243	1.679	0.028	1	0.394	0.537	
	Group		−3.891	−6.512	−1.270	0.002	1	0.023	0.882	
	Interaction		9.986	3.252	16.720	0.685	1	9.567	0.006	**
	Residuals					1.431	20			
Thalamus	**Thalamo-precuneus**	0.296								
	FA		0.852	−1.356	3.060	0.118	1	1.607	0.219	
	Group		−6.133	−11.053	−1.212	0.000	1	0.000	0.999	
	Interaction		16.134	3.197	29.071	0.497	1	6.767	0.017	*
	Residuals					1.468	20			

[a]Statistics and confidence interval of the regression models to predict SUV using FA of adjacent tracts and group (brain-injured patients or patients who recovered the ability to functionally communicate or use objects in a functionl manner). * = $P < 0.05$, ** = $P < 0.01$, *** = $P < 0.00$.

Interestingly, we did not find a structure–function relationship at the global brain level, suggesting that our results do not solely reflect general brain integrity. Instead, the function–structure relationship of the DMN might be directly related to consciousness. This has been shown in single-modality studies, for example functional connectivity [Vanhaudenhuyse et al., 2010b), white matter structural integrity [Fernández-Espejo et al., 2011, 2012; Gomez et al., 2012], and metabolic function [Thibaut et al., 2012]. Here we show for the first time a direct function–structure relationship within this network.

As expected, healthy control subjects showed FA and SUV within normal range and therefore we are unable to make inferences about whether one drives the other. Next we investigated the function–structure relationship within our patient population, comparing EMCS with DOC patients (MCS and UWS). EMCS patients are able to use objects and/or functionally communicate, and thus by definition conscious. Apart from one region-connection pair, all observed main effects of FA seen in the healthy vs. brain injured analysis were also observed in the analysis between the two patient populations, indicating that there is a positive linear relation between functional and structural integrity of the DMN. Furthermore, in contrast to DOC patients, EMCS patients show a significantly stronger function–structure interaction between the function of the thalamus and the structural integrity of the thalamo-inferiorparietal tract. On the uni-modal level our results match previous research in post-comatose patients finding that structural cortico-thalamic connections are diminished [Lant et al., 2015] and thalamic metabolism is lowered [Fridman et al., 2014]. These findings can be explained by the mesocircuit theory, which proposes that large-scale dysfunction is due to a global decrease of excitatory neurotransmission which in turn alters cerebral activity. More specifically, the globus pallidus is disinhibited and overactive, inhibiting the thalamic excitatory output to the frontal cortex [Schiff, 2010]. By combining both functional metabolism and white matter structural information we here provide further evidence for the validity of this theory, supporting the hypothesis that thalamo-cortical connectivity plays an important role in emergence of consciousness [Schiff, 2010]. We limited ourselves to the DMN because of the large body of literature on this brain-network relating to consciousness. Therefore, future research should extend these findings to more specific sub-cortical regions, such as the globus pallidus or specific thalamic regions.

We do not find any difference between patients based on aetiology, even though several studies have shown that temporal dynamics of Wallerian degeneration vary given different aetiologies [Kumar et al., 2009; Luyt et al., 2012] and that traumatic brain injury, unlike anoxia, might selectively affect DMN white matter integrity [Bonnelle et al., 2011; Warner et al., 2010]. Multicentre collaborations should provide sufficiently large datasets to study these effects in the future.

Methodologically, several comments can be addressed when dealing with brain-injured patients, especially concerning normalization, SUV, and tractography procedures. We here chose to perform a within-subject ROI labelling rather than applying a common atlas after spatial normalization as this latter procedure might results in a lack of inter-subject anatomical correspondence in severely injured brains. As there is no consensus on the most

reliable calculation of standard uptake value, we accounted for the partial-volume effect [Rousset et al., 2007]. Tractography based on constrained spherical deconvolution is optimal with b-values of 2,500–3,000 s/mm^2 [Tournier et al., 2013], but crossing fibres can still be more reliably modelled than with simple DTI-based models using our lower b-value of 1,000 s/mm^2 [e.g., see for effective application: Roine et al., 2015]. Future studies should strive to acquire diffusion-weighted images using isotropic voxels, as anisotropic voxel sizes produce datasets in which the fibre orientation estimates depend on the position of the subject in the scanner. Anisotropic voxel sizes were mitigated in this study by linear interpolation of the fibre orientation distributions during the fibre tracking step.

CONCLUSION

We here assessed the function–structure relationship within healthy, conscious subjects and severely brain damaged patients with varying levels of consciousness through direct combined investigation of function (FDG-PET), and structure (MRI-DWI). Levels of structural integrity (FA) and metabolic function (standardized metabolic rates) are significantly diminished in patients compared with controls. Furthermore, a significant positive function–structure relationship can be observed within most regions of the DMN. This relationship may be network-specific, as it does not appear at the whole-brain level. Finally, we show that EMCS compared with DOC show a significantly stronger thalamo-cortical function–structure relationship, which is in line with the mesocircuit hypothesis.

REFERENCES

Boly M, Tshibanda L, Vanhaudenhuyse A, Noirhomme Q, Schnakers C, Ledoux D, Boveroux P, Garweg C, Lambermont B, Phillips C (2009): Functional connectivity in the default network during resting state is preserved in a vegetative but not in a brain dead patient. Hum Brain Mapp 30:2393–2400.

Bonnelle V, Leech R, Kinnunen KM, Ham TE, Beckmann CF, De Boissezon X, Greenwood RJ, Sharp DJ (2011): Default mode network connectivity predicts sustained attention deficits after traumatic brain injury. J Neurosci 31:13442–13451.

Bozoki AC, Korolev IO, Davis NC, Hoisington LA, Berger KL (2012): Disruption of limbic white matter pathways in mild cognitive impairment and Alzheimer's disease: A DTI/FDG-PET Study. Hum Brain Mapp 33:1792–1802.

Chandra PS, Salamon N, Huang J, Wu JY, Koh S, Vinters HV, Mathern GW (2006): FDG-PET/MRI coregistration and diffusion-tensor imaging distinguish epileptogenic tubers and cortex in patients with tuberous sclerosis complex: A preliminary report. Epilepsia 47:1543–1549.

De Volder AG, Bol A, Blin J, Robert A, Arno P, Grandin C, Michel C, Veraart C (1997): Brain energy metabolism in early blind subjects: Neural activity in the visual cortex. Brain Res 750:235–244.

Demertzi A, Gómez F, Crone JS, Vanhaudenhuyse A, Tshibanda L, Noirhomme Q, Thonnard M, Charland-Verville V, Kirsch M, Laureys S, et al. (2014): Multiple fMRI system-level baseline connectivity is disrupted in patients with consciousness alterations. Cortex 52:35–46. doi:10.1016/j.cortex.2013.11.005.

Desikan RS, Ségonne F, Fischl B, Quinn BT, Dickerson BC, Blacker D, Buckner RL, Dale AM, Maguire RP, Hyman BT, et al. (2006): An automated labeling system for subdividing the human cerebral cortex on MRI scans into gyral based regions of interest. Neuroimage 31:968–980. doi:10.1016/j.neuroimage.2006.01.021.

Ennis DB, Kindlmann G (2006): Orthogonal tensor invariants and the analysis of diffusion tensor magnetic resonance images. Magn Reson Med 55:136–146.

Fernández-Espejo D, Bekinschtein T, Monti MM, Pickard JD, Junque C, Coleman MR, Owen AM (2011): Diffusion weighted imaging distinguishes the vegetative state from the minimally conscious state. Neuroimage 54:103–112.

Fernández-Espejo D, Soddu A, Cruse D, Palacios EM, Junque C, Vanhaudenhuyse A, Rivas E, Newcombe V, Menon DK, Pickard JD, et al. (2012): A role for the default mode network in the bases of disorders of consciousness. Ann Neurol 72:335–343.

Fridman EA, Beattie BJ, Broft A, Laureys S, Schiff ND (2014): Regional cerebral metabolic patterns demonstrate the role of anterior forebrain mesocircuit dysfunction in the severely injured brain. Proc Natl Acad Sci USA 111:6473–6478.

Gallichan D, Scholz J, Bartsch A, Behrens TE, Robson MD, Miller KL (2010): Addressing a systematic vibration artifact in diffusion-weighted MRI. Hum Brain Mapp 31:193–202.

Garyfallidis E, Brett M, Amirbekian B, Rokem A, van der Walt S, Descoteaux M, Nimmo-Smith I (2014): Dipy, a library for the analysis of diffusion MRI data. Front Neuroinform 8:8.

Giacino JT, Ashwal S, Childs N, Cranford R, Jennett B, Katz DI, Kelly JP, Rosenberg JH, Whyte J, Zafonte RD, et al. (2002): The minimally conscious state: Definition and diagnostic criteria. Neurology 58:349.

Giacino JT, Kalmar K, Whyte J (2004): The JFK Coma Recovery Scale-Revised: Measurement characteristics and diagnostic utility. Arch Phys Med Rehabil 85:2020–2029. doi:10.1016/j.apmr.2004.02.033.

Gómez F, Soddu A, Noirhomme Q, Vanhaudenhuyse A, Tshibanda L, Lepor N (2012): DTI based structural damage characterization for disorders of consciousness.In: 2012 19th Ieee International Conference on Image Processing, 2:1257–1260.

Gorgolewski K, Burns CD, Madison C, Clark D, Halchenko YO, Waskom ML, Ghosh SS (2011): Nipype: A flexible, lightweight and extensible neuroimaging data processing framework in python. Front Neuroinform 5:1–15.

Greicius MD, Supekar K, Menon V, Dougherty RF (2009): Resting-state functional connectivity reflects structural connectivity in the default mode network. Cereb Cortex 19:72–78. doi:10.1093/cercor/bhn059.

Inoue K, Ito H, Uchida S, Taki Y, Kinomura S, Tsuji I, Sato S, Horie K, Kawashima R, Ito M, et al. (2008): Decrease in glucose metabolism in frontal cortex associated with deterioration of microstructure of corpus callosum measured by diffusion tensor imaging in healthy elderly. Hum Brain Mapp 29:375–384. doi:10.1002/hbm.20394.

Jones DK, Horsfield MA, Simmons A (1999): Optimal strategies for measuring diffusion in anisotropic systems by magnetic resonance imaging. Magn Reson Med 42:515–525.

Jeong JW, Tiwari VN, Shin J, Chugani HT, Juhász C (2015): Assessment of brain damage and plasticity in the visual system due to early occipital lesion: Comparison of FDG-PET with diffusion MRI tractography. J Magn Reson Imaging 41:431–438.

Koay CG (2009): On the six-dimensional orthogonal tensor representation of the rotation in three dimension: A simplified approach. Mech Mater 41:951–953.

Kuczynski B, Targan E, Madison C, Weiner M, Zhang Y, Reed B, Chui HC, Jagust W (2010): White matter integrity and cortical metabolic associations in aging and dementia. Alzheimers Dement 6:1–17. doi:10.1016/j.jalz.2009.04.1228.White.

Kumar R, Husain M, Gupta RK, Hasan KM, Haris M, Agarwal AK, Pandey CM, Narayana PA (2009): Serial changes in the white matter diffusion tensor imaging metrics in moderate traumatic brain injury and correlation with neuro-cognitive function. J Neurotrauma 495:481–495.

Lant ND, Gonzalez-Lara LE, Owen AM, Fernández-Espejo D (2015): Relationship between the anterior forebrain mesocircuit and the default mode network in the structural bases of disorders of consciousness. NeuroImage Clin 10:27–35.

Laureys S, Schiff ND (2012): Coma and consciousness: Paradigms (re)framed by neuroimaging. Neuroimage 61:478–491.

Laureys S, Goldman S, Phillips C, van Bogaert P, Aerts J, Luxen A, Franck G, Maquet P (1999a): Impaired effective cortical connectivity in vegetative state: Preliminary investigation using PET. Neuroimage 9:377–382.

Laureys S, Lemaire C, Maquet P, Phillips C, Franck G (1999b): Cerebral metabolism during vegetative state and after recovery to consciousness. J Neurol Neurosurg Psychiatry 67:121.

Laureys S, Owen AM, Schiff ND (2004): Brain function in coma, vegetative state, and related disorders. Lancet 3:537–546.

Laureys S, Celesia GG, Cohadon F, Lavrijsen J, Leon-Carrrion J, Sannita WG, Sazbon L, Schmutzhard E, von Wild KR, Zeman A, et al. (2010): Unresponsive wakefulness syndrome: A new name for the vegetative state or apallic syndrome. BMC Med 8:68.

Leemans A, Jones DK (2009): The B-matrix must be rotated when correcting for subject motion in DTI data. Magn Reson Med 61:1336–1349.

Luyt CE, Galenaud D, Perlbarg V, Vanhaudenhuyse A, Stevens RD, Gupta R, Besancenot H, Krainik A, Audibert G, Combes A, et al. (2012): Diffusion tensor imaging to predict long-term outcome after cardiac arrest. Anesthesiology 117:3–1.

Müller-Gärtner HW, Links JM, Prince JL, Bryan RN, McVeigh E, Leal JP, Davatzikos C, Frost JJ (1992): Measurement of radiotracer concentration in brain gray matter using positron emission tomography: MR-based correction for partial volume effects. J Cereb Blood Flow Metab 12:571–583.

Nakashima T, Nakayama N, Miwa K, Okumura A, Soeda A, Iwama T (2007): Focal brain glucose hypometabolism in patients with neuropsychologic deficits after diffuse axonal injury. Am J Neuroradiol 28:236–242. [pii].

Nakayama N, Okumura A, Shinoda J, Nakashima T, Iwama T (2006): Relationship between regional cerebral metabolism and consciousness disturbance in traumatic diffuse brain injury without large focal lesions: An FDG-PET study with statistical parametric mapping analysis. J Neurol Neurosurg Psychiatry 77:856–862.

Quarantelli M, Berkouk K, Prinster A, Landeau B, Svarer C, Balkay L, Alfano B, Brunetti A, Baron JC, Salvatore M (2004): Integrated software for the analysis of brain PET/SPECT studies with partial-volume-effect correction. J Nucl Med 45: 192–201.

R core team (2014): R: A Language and Environment for Statistical Computing. Vienna, Austria: Statistical Computing. URL: https://www.R-project.org

Roine U, Salmi J, Roine T, Wendt TN, Leppämäki S, Rintahaka P (2015): Constrained spherical deconvolution-based tractography and tract-based spatial statistics show abnormal microstructural organization in Asperger syndrome. Mol Autism 6:4.

Rousset O, Rahmim A, Alavi A, Zaidi H (2007): Partial volume correction strategies in PET. PET Clin 2:235–249.

Rudolf J, Ghaemi M, Haupt WF, Szelies B, Heiss WD (1999): Cerebral glucose metabolism in acute and persistent vegetative state. J Neurosurg Anesthesiol 11:17–24.

Schiff NDN (2010): Recovery of consciousness after brain injury: A mesocircuit hypothesis. Trends Neurosci 33:1–9.

Smith SM, Jenkinson M, Woolrich MW, Beckmann CF, Behrens TEJ, Johansen-Berg H, Bannister PR, De Luca M, Drobnjak I, Flitney DE, et al. (2004): Advances in functional and structural MR image analysis and implementation as FSL. Neuroimage 23:208.

Soddu A, Vanhaudenhuyse A, Bahri MA, Bruno MA, Boly M, Demertzi A, Tshibanda JF, Phillips C, Stanziano M, Ovadia-Caro S, et al. (2012): Identifying the default-mode component in spatial IC analyses of patients with disorders of consciousness. Hum Brain Mapp 33:778–796. doi:10.1002/hbm.21249.

Stender J, Gosseries O, Bruno MA, Charland-Verville V, Vanhaudenhuyse A, Demertzi A, Chatelle C, Thonnard M, Thibaut A, Heine L, et al. (2014a): Diagnostic precision of PET imaging and functional MRI in disorders of consciousness: A clinical validation study. Lancet 384:514–522.

Stender J, Kupers R, Rodell A, Thibaut A, Chatelle C, Bruno MA, Gejl M, Bernard C, Hustinx R, Laureys S, et al. (2014b): Quantitative rates of brain glucose metabolism distinguish minimally conscious from vegetative state patients. J Cereb Blood Flow Metab 35:58.

Svarer C, Madsen K, Hasselbalch SG, Pinborg LH, Haugbøl S, Frøkjær VG, Holm S, Paulson OB, Knudsen GM (2005): MR-based automatic delineation of volumes of interest in human brain PET images using probability maps. Neuroimage 24:969–979.

Thibaut A, Bruno M (2012): Metabolic activity in external and internal awareness networks in severely brain-damaged patients. J Rehabil Med 44:487–494.

Thibaut A, Bruno MA, Chatelle C, Gosseries O, Vanhaudenhuyse A, Demertzi A, Schnakers C, Thonnard M, Charland-Verville V, Bernard C, et al. (2012): Metabolic activity in external and internal awareness networks in severely brain-damaged patients. J Rehabil Med 44:481–516.

Tommasino C, Grana C, Lucignani G, Torri G, Fazio F (1995): Regional cerebral metabolism of glucose in comatose and vegetative state patients. J Neurosurg Anesthesiol 7:109–116.

Tournier JD, Calamante F, Connelly A (2012): MRtrix: Diffusion tractography in crossing fiber regions. Int J Imaging Syst Technol 22:53–66.

Tournier JD, Calamante F, Connelly A (2013): Determination of the appropriate b value and number of gradient directions for high-angular-resolution diffusion-weighted imaging. NMR Biomed 26:1775–1786.

Van Den Heuvel MP, Mandl RCW, Kahn RS, Hulshoff Pol HE (2009): Functionally linked resting-state networks reflect the underlying structural connectivity architecture of the human brain. Hum Brain Mapp 30:3127–3141.

Vanhaudenhuyse A, Demertzi A, Schabus M, Noirhomme Q, Bredart S, Boly M, Phillips C, Soddu A, Luxen A, Moonen G (2010a): Two distinct neuronal networks mediate the awareness of environment and of self. J Cogn Neurosci 23:570–578.

Vanhaudenhuyse A, Noirhomme Q, Tshibanda LJF, Bruno MA, Boveroux P, Schnakers C, Soddu A, Perlbarg V, Ledoux D, Brichant JF (2010b): Default network connectivity reflects the level of consciousness in non-communicative brain-damaged patients. Brain 133:161–171.

Warner MA, Youn TS, Davis T, Chandra A, Marquez de la Plata C, Moore C, Harper C, Madden CJ, Spence J, McColl R, et al. (2010): Regionally selective atrophy after traumatic axonal injury. Arch Neurol 67:1336–1344.

Yakushev I, Schreckenberger M, Müller MJ, Schermuly I, Cumming P, Stoeter P, Gerhard A, Fellgiebel A (2011): Functional anatomy of interhemispheric cortical connections in the human brain. Eur. J Nucl Med Mol Imaging 38:2219–2227.

Yakushev I, Chételat G, Fischer FU, Landeau B, Bastin C, Scheurich A, Perrotin A, Bahri MA, Drzezga A, Eustache F, et al. (2013): Metabolic and structural connectivity within the default mode network relates to working memory performance in young healthy adults. Neuroimage 79:184–190.